# Morphological classification and quantitative analysis of etch pits

C. Motzer and M. Reichling[a)]

*Fachbereich Physik, Universität Osnabrück, Barbarastr. 7, 49069 Osnabrück, Germany*

Etch pits created by hydrochloric and phosphoric acid on cleaved $CaF_2(111)$ are investigated by scanning force microscopy (SFM). A geometric and dimensional analysis of the etch pits reveals two distinctly different types. Type-I etch pits evolve at dislocation defects, are pointed and their size and eccentricity is related to the angle between the dislocation and the surface. Type-II etch pits result from defects below the surface, are flat-bottomed for longer etching times and exhibit a characteristic ratio of depth and edge length depending on the type of etchant. An analysis of etch pit morphology allows an identification of the origin of an etch pit and a characterization of the associated defect structure. © *2010 American Institute of Physics.* [doi:10.1063/1.3510535]

## I. INTRODUCTION

Highest quality fluorite ($CaF_2$) is an important material for numerous optical applications. For instance, it is used for low chromatic aberration lens systems,[1] it is important as a window material for high power lasers[2] and has widespread applications as a lens material for lithography in the deep ultraviolet (DUV) spectral region.[3] Fluorite is the only material suitable for vacuum ultraviolet lithography due to its large band gap and small birefringence.[3] Recently, highly nonlinear processes in fluorite have extensively been studied establishing fluorite as a key material also in ultrashort laser pulse systems for white light generation and parametric amplification.[4–6] However, advanced applications of fluorite as a bulk optical material are limited by intrinsic birefringence,[7] intrinsic defects,[8,9] and irradiation created nanoparticles,[10,11] impurities,[12] and imperfections in the crystal structure like dislocations[13] that may strongly interact with laser light.[14] At the surface, step edges[15] as well as polishing artifacts[16,17] may reduce the optical performance.[18]

Etching the surface and determining the etch pit density (EPD) is a standard method of determining the quality of $CaF_2$ crystals[19–21] as it probes some of the defects mentioned above. Etch pits are usually detected by optical or electron microscopy and the EPD is regarded as a figure of merit of the material. Recently, we demonstrated for the example of etching the $CaF_2(111)$ surface that scanning force microscopy (SFM) is not only able to detect and count minute etch pits but also allows for their precise characterization in the micrometer and nanometer scales.[22] The method has shown its strength also for a detailed investigation of dislocations in fluorite that are parts of extended networks formed as boundaries between subgrains in imperfect material,[23] for an analysis of complex etch figures giving access to subgrain detail structures related to creep and plasticity behavior[22,24] and for the detection and quantification of deformation related defects that occur in nanoindentation testing.[25]

Here, we investigate in detail individual etch pits on (111) fluorite cleavage plates by high resolution AFM inspection where we aim to relate the apparent morphological char-acteristics and dimensional properties of etch pits to the origin of preferential etching at a local defect. As we identified phosphoric acid and hydrochloric acid as those acids among others investigated that produce etching features best suited for a quantitative analysis,[22] we use these etchants throughout the present study. Figures 1(a) and 1(b) provide an overview of typical etching results and in Figs. 1(c) and 1(d), we introduce the basic morphologies and notation to describe the structure of etch pits. In the AFM image of Fig. 1(a), we find *pointed* ($\alpha$ and $\beta$) and *flat-bottomed etch pits* ($\delta$) that
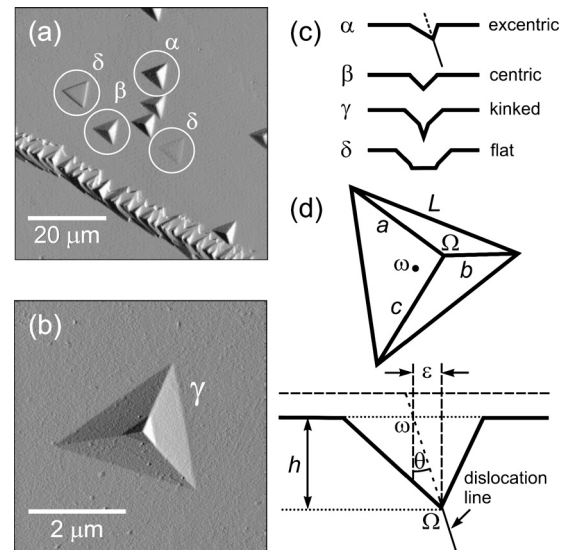


FIG. 1. (a) Illustration of different types of etch pits for the example of etching $CaF_2(111)$ with 2.3*M* HCl (4 min at 25 °C). AFM investigation allows a clear identification of pointed ($\alpha$ and $\beta$) and flat-bottomed ($\delta$) etch pits. Etch pits may either be eccentric ($\alpha$) or centric ($\beta$). (b) Etch pit with a kinked-wall created by etching $CaF_2(111)$ with 10*M* $H_3PO_4$ (10 min at 100 °C). (c) Classification of etch pit morphology for the examples shown in frames (a) and (b). (d) Schematic representation of an eccentric pointed etch pit in top view (upper) and a cross-sectional view along a plane perpendicular to the surface including the root point $\Omega$ of the etch pit and the triangle centroid $\omega$ (lower). The etch pit is bound by an equilateral triangle with a side length $L$ and has three inner ledges with lengths $a \neq b \neq c$. The length of the projection of a line connecting points $\Omega$ and $\omega$ onto the surface plane is the eccentricity $\varepsilon$. The angle $\theta$ enclosed by the dislocation line and the surface normal can be calculated from the depth $h$ of the etch pit and its eccentricity $\varepsilon$.

a)Electronic mail: reichling@uos.de.

may be *eccentric* ($\alpha$) or *centric* ($\beta$). Most important for understanding etching related to localized defects are etch pits having *kinked*-walls as exemplified in etch pit $\gamma$ of Fig. 1(b). As a main result of this study, we demonstrate that a detailed geometric analysis of etch pits allows a further differentiation between two types of etch pits, namely *type-I* and *type-II* etch pits independent of their appearance as pointed or flat-bottomed. While type-I defects are related to dislocations terminating at the surface, type-II defects are solely related to localized subsurface defects. The dimensions and depth of a subsurface defect in conjunction with the etching duration determines whether or not a pointed etch pit will evolve into a flat-bottomed one.

## II. EXPERIMENTAL DETAILS

Experiments are performed on pristine (111) surfaces of $CaF_2$ crystals obtained by cleavage of a single crystal rod of the highest quality available (DUV grade) with $20 \times 20$ mm$^2$ cross-section (Korth Kristalle GmbH, Kiel, Germany) under normal conditions. Cleavage plates of typically 2 mm thickness are etched by immersing them in the etch bath that contains either 2.3$M$ hydrochloric acid or concentrated phosphoric acid for a well-defined time without agitation of the media. Samples etched with phosphoric acid are briefly dipped into nitric acid after the main etching step to remove precipitates formed by the weakly soluble salt of phosphoric acid.[22] In a last preparation step, samples are rinsed with distilled water and dried with lint-free paper. SFM investigations of the etch pits are performed with a commercial force microscope operated in the contact mode (easyScan, Nanosurf AG, Liestal, Switzerland). Images represent surfaces scanned from left to right in the slow scanning direction from bottom to top and are displayed after having passed a derive filter encoding the slope of the surface in gray scale values. Dark areas are descending and bright areas are ascending in topography when related to the fast scanning direction.

## III. RESULTS

Etching the (111) cleavage face of fluorite in the vicinity of defects results in the formation of etch pits that are mostly equilateral triangles with edges parallel to [110] and equivalent directions due to the threefold symmetry of $CaF_2$(111).[22] Most of the etch pits have a clearly defined root point at the bottom marked as $\Omega$ in the schematic description introduced in Fig. 1(d). *Pointed etch pits* are in general eccentric where the root point $\Omega$ of the etch pit is displaced from the triangle center $\omega$ by the eccentricity $\varepsilon$ caused by the inclination of the original dislocation line. From the analysis of SFM images, we can determine the length $L$ of the etch pit edges, the etch pit height $h$ and the length of the inner edges $a$, $b$, and $c$. The angle $\theta$ is defined as the angle between the dislocation and the surface normal.

For a quantitative geometric analysis, we first investigate the relation between the depth $h$ and the dislocation angle $\theta$ of the etch pit. To derive a characteristic geometric parameter describing the etch pit regardless of its state of evolution, we define a flatness parameter $f$ relating the etch pit height $h$ to the edge length $L$ as

$$f = \frac{L}{h}.$$

Furthermore, the eccentricity $\varepsilon$ is determined by length measurements of the three inner edges $a$, $b$, and $c$. The triangle from Fig. 1(b) is overdetermined by the parameters $a$, $b$, $c$, and $L$ and, therefore, we calculate the eccentricity from the length of two inner edges and $L$ and use the third one for an error check

$$\varepsilon = \sqrt{\left(\frac{a^2 - b^2}{2L}\right)^2 + \left\{\frac{L}{2\sqrt{3}} - \frac{1}{2L}\sqrt{[(a+b)^2 - L^2][L^2 - (b-a)^2]}\right\}^2}.$$

The inclination $\theta$ of the dislocation against the surface normal is determined by relating the eccentricity to the height of the etch pit

$$\theta = \tan^{-1}\left(\frac{\varepsilon}{h}\right).$$

With this parameterization, we are able to determine the inclination $\theta$ of the dislocation from quantitatively analyzing the apparent shape of the related etch pit and can deduce a relation between the inclination $\theta$ and the flatness $f$ of the etch pit.

We first analyze *pointed etch pits* having *straight walls* and clearly identify two types, namely eccentric etch pits, further on referred to as *type-I etch pits* and centric etch pits, further on referred to as *type-II etch pits*. These two types yield distinctly different etching results regardless of the applied acid and other etching parameters. They can be distinguished from each other not only by their symmetry properties but also by their flatness that is a monotonous function of $\theta$ for type-I etch pits. As will be argued below, type-II etch pits are not simply a special case of type-I etch pits with a small dislocation angle but rather they represent an independent class of etch pits having a different origin. In Fig. 2, we investigate the relation between the flatness $f$ and the dislocation inclination $\theta$ for a large number of *type-I etch pits* for the two acids investigated. For both acids, we find the same result qualitatively, namely, the flatness strongly increases for the inclination approaching 90° while it converges to a certain value $f_I$ for a vanishing inclination $\theta$ that is 22 for phosphoric acid and 28 for hydrochloric acid. Notably, the data in the graphs of Fig. 2 significantly scatters around an ideal line indicating a large statistical measurement error on first sight. A closer look at the data, however, reveals that deviations are systematic for the individual etch pit and originate from bends in the walls of etch pits. This is not surprising since it is well known that dislocation lines which are the origin of the etch pits may have a curvature.[26] In fact, straight dislocation lines are an idealized assumption and naturally the probability of finding a deviation from the straight line increases with the depth of the etch pit. Hence, it is difficult to find deep etch pits having no curvature in their shape. We also analyze a number of *type-II etch pits* and find a flatness of $f_{II} = 26 \pm 2$ for phosphoric acid and $f_{II} = 50 \pm 2$
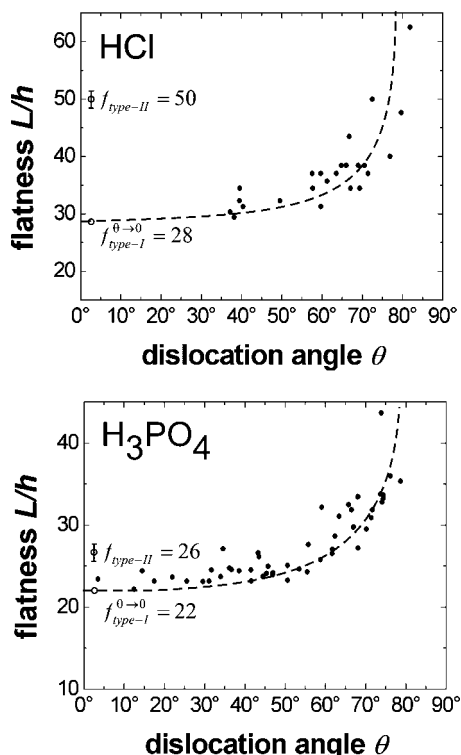
FIG. 2. The angle $\theta$ between the dislocation line and the surface normal plotted against the flatness $f$ for eccentric (type-I) pointed etch pits as derived from a large number of etching experiments with 2.3$M$ HCl (upper graph) and conc. $H_3PO_4$ (lower graph). Dots represent results from an analysis of individual etch pits while the dashed lines serve as a guide for the eye indicating the unknown functional relationship. The flatness diverges for the inclination angle approaching 90° while it approaches a value of 28 for HCl and 22 for $H_3PO_4$ for the dislocation angle approaching 0°. For comparison, the respective flatness values of 50 for HCl and 26 for $H_3PO_4$ found for centric (type-II) etch pits are included in the graph.

for hydrochloric acid. The respective values are significantly different from the small $\theta$ limit of type-I etch pits and are included in Fig. 2 as single points. This demonstrates that type-I and type-II etch pits can be discriminated unambiguously even if the inclination of the former is very small. The basic difference is that type-II etch pits are always centric and flatter than type-I etch pits regardless of the type of etch solution, however, the ratio of the flatness parameters $f_I$ and $f_{II}$ depends on the etchant.

By complete analogy with the findings for straight-wall etch pits, we describe properties of *kinked-wall etch pits*. The structural characteristic of this class of etch pits is that their confining walls have two different slopes where the slope in the lower part of the etch pit is mostly steeper than in the upper part. Kinked-wall etch pits may appear as pointed [see Fig. 1(b)] or with a flat bottom [see $\delta$ in Fig. 1(a)]; the latter are referred to later as *flat pits*. The lower part of a kinked-wall etch pit is referred to as the *pot* and we find that the walls are generally rougher in the pot region than for the region above the kink. This description as a pot is most evident for fully developed flat pits, however, the pot is not always easy to be identified as it may be very narrow, it may have a small height or the wall above the kink may be very narrow depending on the state of the development of the etch pit. The general structure and nomenclature for the quantita-
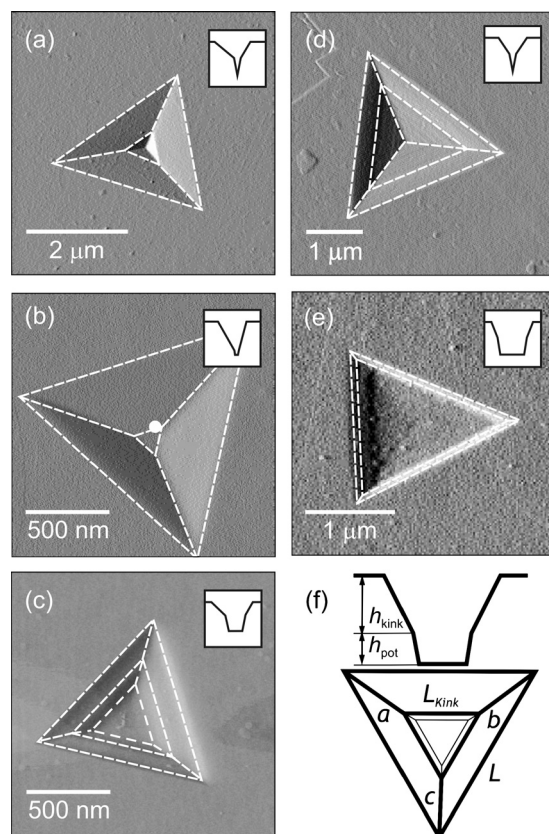


FIG. 3. [(a)–(e)] Representative etching results for type-I [(a) to (c)] and type-II [(d) and (e)] kinked-wall etch pits resulting from etching $CaF_2$(111) with HCl and $H_3PO_4$, respectively. (a) Transition of a pointed etch pit to a flat pit by etching with conc. $H_3PO_4$ (10 min at 100 °C). Parameters: $L$ =3.28 $\mu$m, $L_{kink}$=0.78 $\mu$m, $h_{kink}$=116 nm, and $h_{pot}$=91 nm, inner edges $a$, $b$, and $c$ are 1.42 $\mu$m, 1.39 $\mu$m, and 1.45 $\mu$m, respectively, $\theta$=25°, the flatness of $f$=22 is typical for eccentric type-I etch pits. (b) Type-I etch pit with a flat bottom by etching with conc. $H_3PO_4$ (120 min at 50 °C). Parameters: $L$=1.39 $\mu$m, $L_{kink}$=170 nm, $h_{kink}$=36.2 nm, and $h_{pot}$=4 nm, inner edges $a$, $b$, and $c$ are 736 nm, 773 nm, and 634 nm, respectively, $\theta$=66°, $f$=33. The white dot is the geometric center $\omega$. There is an unevenness at the bottom pointing to a localized defect that presumably has been the pinning center of the dislocation line. Due to its small height, the pot is hardly visible. (c) Type-I flat pit etched by conc. $H_3PO_4$ (20 min at 90 °C) with a clearly discernible pot. Parameters: $L$=4.72 $\mu$m, $L_{kink}$=2.73 $\mu$m, $h_{kink}$ =30 nm, and $h_{pot}$=25 nm, inner edges $a$, $b$, and $c$ are 1.06 $\mu$m, 1.17 $\mu$m, and 0.96 $\mu$m, respectively, $\theta$=85° and $f$=67. The flatness points to a very large eccentricity. (d) Transition state from a pointed etch pit to a flat pit by etching with 2.3$M$ HCl (4 min at 25°). Parameters: $L$=3.07 $\mu$m, $L_{kink}$ =1.95 $\mu$m, $h_{kink}$=40 nm, and $h_{pot}$=39 nm, inner edges $a$, $b$, and $c$ are each 645 nm, and $f$=48. The centric appearance together with the typical flatness identify the etch pit as type-II. (e) Type-II flat pit by etching with 2.3$M$ HCl (2 min at 21 °C) with a laterally extended pot. Parameters: $L$=2.20 $\mu$m, $L_{kink}$=1.69 $\mu$m, $h_{kink}$=10 nm, and $h_{pot}$=9.1 nm, inner edges $a$, $b$, and $c$ are each 250 nm, and $f$=51. The small value for $h_{kink}$ indicates that the defect creating the etch pit was close to the surface. (f) Schematic representation of an eccentric flat pit introducing the notation for the depth of the pot $h_{pot}$, the size of the upper part of the etch pit wall $h_{kink}$ and the length of the inner ledges $L_{kink}$ together with a redefinition of other relevant length parameters by analogy with Fig. 1(c).

tive analysis of kinked-wall etch pits is illustrated schematically in Fig. 3(f). We can also discriminate eccentric type-I and centric type-II etch pits for flat pits. Figures 3(a)–3(c) is a compilation of representative images of type-I flat pits having different characteristics. For the pointed etch pit shown in Fig. 3(a), the pot is barely developed but can be identified by a careful inspection of the kink in the etch pit walls. A
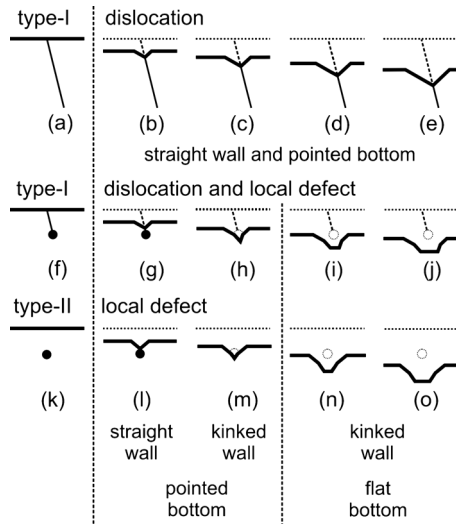
FIG. 4. Schematic representation of the structure of straight wall [frames (a) to (e)] and kinked-wall [frames (f) to (o)] etch pits as they develop with etching time. The left column represents the initial situation before etching. The level of the original surface before etching is indicated by dashed horizontal lines in snapshots taken later during progressive etching (from left to right). The solid and dashed slanted lines indicate a present dislocation line and the position of a vanished dislocation line, respectively, while black dots and dashed circles indicate present and vanished localized defects. [(a)–(e)] Structure of an eccentric pointed etch pit caused by a dislocation breaking through the surface. [(f)–(j)] Structure of an eccentric flat pit caused by the combination of a dislocation and a localized defect. [(k)–(o)] Structure of a centric flat pit caused by a localized defect.

noncentric bottom plateau is clearly developed for the etch pit shown in Fig. 3(b), however, its pot has a height of only 4 nm compared to the kink height of 36 nm so that here too, the pot can barely be identified. In Fig. 3(c), we present a flat pit with a well-developed large pot that is 25 nm high. Figures 3(d) and 3(e) show type-II flat pits of a different character. The etch pit shown in Fig. 3(d) is again a pointed etch pit with kinked walls but is fully centric. On the other hand, the centric etch pit shown in Fig. 3(e) exhibits a large flat bottom but only a small pot height so that the second kink in the etch pit walls is just barely visible. For a quantitative analysis of kinked-wall etch pits, the formal description as developed for the straight wall etch pits is adapted to the geometrical specifics of the kinked walls. In addition to the length $L$ of the outer ledges of the etch pit, we measure the length of the kink separating the wall regions of different slope as $L_{kink}$ [see Fig. 3(f)] and define a length increment $\Delta L = L - L_{kink}$. For reasons outlined in the interpretation developed below, it is reasonable to define the flatness parameter $f$ for flat pits as

$$f = \frac{L - L_{kink}}{h_{kink}} = \frac{\Delta L}{h_{kink}}.$$

With this definition, we find a variable flatness for type-I kinked-wall and flat pits and values that are compatible with those determined from pointed etch pits for type-II flat pits.

We now develop a model explaining the different morphologies of the etch pits by reason of their origin from a dislocation line, a local defect or a combination of both. A summary of the interpretation is given in the schematic drawings compiled in Fig. 4 where we contrast structures for

straight-wall etch pits with structures for the two types of kinked-wall etch pits. While the left column [sketches (a), (f), and (k)] shows the initial situation with a solid, inclined line symbolizing a dislocation and a dot symbolizing a subsurface defect, the series of further sketches drawn from left to right indicate a temporal progression during the etching period. The shape and size development of straight-wall etch pits [Fig. 4(a)] that originate from dislocations can be explained straightforwardly along the lines outlined in our previous study.[22] Depth and lateral dimension of the pointed etch pit linearly increase as a function of etching time where the ratio, i.e., the flatness parameter $f$ is a constant determined by the etchant (ratio of lateral and vertical etching speed) and the inclination $\theta$ of the dislocation line. Therefore, the shape of the pointed etch pit does not change during etching but the structure grows as a function of the etching time [Figs. 4(b)–4(e)]. Furthermore, the entire surface is etched during exposure to the etchant, and therefore, the actual surface (dashed horizontal line in Fig. 4) moves away from the position of the original surface (solid horizontal line in Fig. 4) during progressive etching.

To explain the structure of kinked-wall etch pits, we propose that they are initiated by a localized defect beneath the original surface [Figs. 4(f), 4(g), 4(k), and 4(l)]. The characteristic change in slope of the etch pit wall indicates that there is a distinct change in the etching behavior at a certain point of the etching process. We associate this change with the presence of the defect buried underneath the surface. During the etching process, the change occurs at the moment where the etching front reaches the defect that is removed by this process [Figs. 4(h) and 4(m) and Figs. 3(a) and 3(d)]. The dimension of the upper part of the etch pit wall created during the initial phase of etching $h_{kink}$ [see Fig. 3(f)] is, therefore, related to the depth of the defect below the original surface. For example, a quantitative analysis of etch pits marked as $\delta$ in Fig. 1(a) would allow us to determine the different depth of the defects causing these flat pits. The formation of the pot and specifically its final height $h_{pot}$ [see Fig. 3(f)] is determined by the etching behavior in the vicinity of the defect that, in turn, depends on the nature and extension of the defect that may be very localized or have a certain extension [Figs. 4(i) and 4(n) and Figs. 3(b) and 3(c)]. Our technique cannot reveal any details of such defects but we speculate that they include single impurities, impurity clusters and small dislocation loops or vacancy clusters[27,28] as we find the pot height ranges from 1 to 90 nm. The large range of pot sizes found points to extended defect structures as a major source for etch pits. As we investigate fluorite material of highest quality with an extremely small content of impurities,[12] dislocation loops appear as the most probable origin for pot formation. This interpretation is supported by the observation of a significantly increased roughness of the etch pit walls in the pot region as etching in a region characterized by the complicated stress field of a dislocation loop is likely to produce inhomogeneity and instability of the etching process.

Within this model, the different behavior of type-I and type-II kinked-wall etch pits is explained by the involvement or noninvolvement of a dislocation in the formation of the

etch pit. Dislocations involved in the formation of type-I kinked-wall etch pits result in eccentricity while type-II kinked-wall etch pits grow as a centric structure with the defect being the central nucleus. Once the defect is removed, both types of kinked-wall etch pits grow exclusively in their lateral dimension as the vertical etching speed in the surroundings of the etch pit is equal to the vertical etching speed for the bottom plateau of the etch pit[22] [Figs. 4(i), 4(j), 4(n), and 4(o) and Fig. 3(e)]. This implies that the edge length $L$ of the flat pit extends at the same pace as the inner edge length $L_{kink}$ [see Fig. 3(f)]. Hence, the difference between $L$ and $L_{kink}$ of a flat pit provides the edge length at the moment of the pot being formed and reflects the state of etching when the dislocation and/or defect is present. Therefore, $\Delta L = L - L_{kink}$ is the appropriate length to be used for the calculation of the flatness parameter $f$ for kinked-wall etch pits by analogy with the definition for the straight-wall etch pits. From this definition it follows that the flatness value of a type-I kinked-wall etch pit is the same as for a straight-wall etch pit for a given dislocation angle $\theta$.

## IV. DISCUSSION AND CONCLUSIONS

To discuss our findings in the context of previous etching studies on fluorite, we note that the development of flat-bottomed etch pits has often been associated incorrectly with the presence of localized defects (see, for instance, Ref. 29). Our detailed analysis reveals that defects but also a combination of a defect with a dislocation line result in the formation of a kinked-wall etch pit that develops into a flat pit after prolonged etching but appears pointed in the early stages of etching. Our observations of different types of etch pits explain findings by MacInnis and Brantley[30] who distinguish two etch pit types by the development of their lateral sizes during dissolution. In their experiments, one type of etch pits transforms more quickly into a flat-bottomed etch pit than the other. In view of our model, the fast ones are type-II etch pits since a subsurface defect causes etch pit formation only if it is reasonably close to the surface while the slower transformation of type-I etch pits can be explained by a long dislocation line. Our model can also explain other indirect evidence for type-II etch pits found in literature in studies of etch figures on opposite cleavage plates. Since dislocations are linear defects, it is highly probably that cleavage will cause similar pointed etch pits at both cleavage faces.[26,31] Patel and Desai,[32] however, reported that this correspondence is not true for small etch pits and flat pits which is easily explained by our interpretation of type-II etch pits being associated with a local defect that is present on only one of the cleavage faces.

The classification of etch pits and the method of their quantitative analysis introduced here are a significant step forward in the analysis of etching results and reach far beyond the classic method of determining the EPD. The method allows for a discrimination between etch pit forma-

tion due to a dislocation, a subsurface defect or a combination of both. In the case of straight-wall etch pits, the angle of inclination between the dislocation line and the surface can be determined and irregularities of the dislocation line can be detected. In the case of kinked-wall etch pits, the position of a defect below the original surface can be determined and the extension of the defect at least estimated from the size of the associated pot. The classification introduced here is not limited to etch pits on fluorite but is also helpful for the characterization of other industrial single crystal materials commonly inspected by etching analysis such as silicon[33] and gallium nitride.[34]

[1] M. Zając and J. Nowak, Optik (Stuttgart) **113**, 299 (2002).
[2] C. A. Klein, J. Appl. Phys. **100**, 083101 (2006).
[3] M. Rothschild, Mater. Today **8**, 18 (2005).
[4] I. Buchvarov, A. Trifonov, and T. Fiebig, Opt. Lett. **32**, 1539 (2007).
[5] I. S. Grudinin, N. Yu, and L. Maleki, Opt. Lett. **34**, 878 (2009).
[6] T. K. Allison, J. van Tilborg, T. W. Wright, M. P. Hertlein, R. W. Falcone, and A. Belkacem, Opt. Express **17**, 8941 (2009).
[7] J. H. Burnett, Z. H. Levine, and E. L. Shirley, Phys. Rev. B **64**, 241102 (2001).
[8] R. Lindner, M. Reichling, R. T. Williams, and E. Matthias, J. Phys.: Condens. Matter **13**, 2339 (2001).
[9] M. Letz, L. Parthier, A. Gottwald, and M. Richter, Phys. Rev. B **67**, 233101 (2003).
[10] M. Reichling, R. M. Wilson, R. Bennewitz, R. T. Williams, S. Gogoll, E. Stenzel, and E. Matthias, Surf. Sci. **366**, 531 (1996).
[11] L. P. Cramer, S. C. Langford, and J. T. Dickinson, J. Appl. Phys. **99**, 054305 (2006).
[12] J. Sils, S. Hausfeld, W. Clauß, U. Pahl, R. Lindner, and M. Reichling, J. Appl. Phys. **106**, 063109 (2009).
[13] A. R. Patel and C. C. Desai, Z. Kristallogr. **121**, 55 (1965).
[14] B. Qian, J. Song, G. P. Dong, L. B. Su, B. Zhu, X. F. Liu, S. Z. Sun, Q. Zhang, and J. R. Qiu, Opt. Express **17**, 8552 (2009).
[15] V. E. Puchin, A. V. Puchina, M. Huisinga, and M. Reichling, J. Phys.: Condens. Matter **13**, 2081 (2001).
[16] S. Gritschneder, Y. Namba, and M. Reichling, Nanotechnology **16**, 883 (2005).
[17] J. Wang and R. L. Maier, Appl. Opt. **45**, 5621 (2006).
[18] S. Gogoll, E. Stenzel, H. Johansen, M. Reichling, and E. Matthias, Nucl. Instrum. Methods Phys. Res. B **116**, 279 (1996).
[19] W. Kleber, M. Hahnert, and I. Lüdtke, Krist. Tech. **1**, 585 (1966).
[20] K. Sangwal, C. C. Desai, and V. John, Krist. Tech. **14**, 63 (1979).
[21] I. Nicoară, O. F. G. Aczel, D. Nicoară, and Z. Schlett, Cryst. Res. Technol. **21**, 647 (1986).
[22] C. Motzer and M. Reichling, J. Appl. Phys. **105**, 064309 (2009).
[23] P. Eisenlohr, P. Sadrabadi, and W. Blum, J. Mater. Sci. **43**, 2700 (2008).
[24] P. Sadrabadi, P. Eisenlohr, G. Wehrhan, J. Stäblein, L. Parthier, and W. Blum, Mater. Sci. Eng., A **510–511**, 46 (2009).
[25] P. Sadrabadi, K. Durst, M. Göken, and W. Blum, Philos. Mag. Lett. **89**, 391 (2009).
[26] A. Sagar and J. W. Faust, Jr., J. Appl. Phys. **38**, 2240 (1967).
[27] I. E. Talanin and V. I. Talanin, Poverkhnost, 66 (2006).
[28] P. J. Roksnoer and M. M. B. van den Boom, J. Cryst. Growth **53**, 563 (1981).
[29] I. Sunagawa, in *Morphology of Crystals: Part A: Fundamentals*, edited by I. Sunagawa (Terra Scientific, Tokyo, 1987), p. 323.
[30] I. N. MacInnis and S. L. Brantley, Chem. Geol. **105**, 31 (1993).
[31] V. H. Babu and K. G. Bansigir, J. Appl. Phys. **40**, 4306 (1969).
[32] A. R. Patel and C. C. Desai, Acta Cryst. **18**, 373 (1965).
[33] M. S. Kulkarni, Ind. Eng. Chem. Res. **42**, 2558 (2003).
[34] X. Xu, R. P. Vaudo, J. Flynn, and G. R. Brandes, J. Electron. Mater. **31**, 402 (2002).